



## **Safety margin for Li-plating-free fast-charging of Li-ion batteries considering parameter uncertainty**

Downloaded from: <https://research.chalmers.se>, 2024-10-26 12:15 UTC

Citation for the original published paper (version of record):

Cai, Y., Li, Y., Wik, T. (2024). Safety margin for Li-plating-free fast-charging of Li-ion batteries considering parameter uncertainty. 2024 IEEE Conference on Control Technology and Applications, CCTA 2024: 722-728. <http://dx.doi.org/10.1109/CCTA60707.2024.10666522>

N.B. When citing this work, cite the original published paper.

© 2024 IEEE. Personal use of this material is permitted. Permission from IEEE must be obtained for all other uses, in any current or future media, including reprinting/republishing this material for advertising or promotional purposes, or reuse of any copyrighted component of this work in other works.

# Safety Margin for Li-Plating-Free Fast-Charging of Li-Ion Batteries Considering Parameter Uncertainty

Yao Cai, Yang Li, and Torsten Wik

**Abstract**—The widespread adoption of electric vehicles has led to increasing concerns about range anxiety. Fast charging of the lithium-ion battery is an important part of addressing this problem. However, a higher charging rate also tends to cause more rapid degradation and shorter battery life. Therefore, how to charge as fast as possible while not leading to excessive aging has become an important research topic. This paper introduces a single particle model-based inversion-based fast charging method with a calculated safety margin. The inversion-based fast-charging method relies a lot on the accuracy of the model parameters that cannot be identified precisely due to inevitable differences between the model and the plant. Provided with the range of parameter uncertainty, a theoretical Li-plating safety margin is calculated with which lithium-plating can be completely avoided. Simulation results demonstrate the effectiveness of the proposed algorithm.

## I. INTRODUCTION

Electric vehicles (EVs) play an important role in the increasing demand for sustainable transportation. On the road to fully displacing fossil-fuelled vehicles, one of the main difficulties to conquer is speeding up the charging process of EV batteries. Charging at excessively high rates is a major cause of accelerated battery degradation, due to the occurrence of lithium-plating and growth of the solid electrolyte interface layers. With the battery's state of health worsened, not only the capacity of the battery is lost, but there is also an increasing risk of safety problems such as internal short circuits and thermal runaways [1]. This can especially happen if a fixed, empirical fast charging protocol is applied, such as constant-current constant-voltage (CCCV) and constant-power CV (CP-CV) methods [2], during which the internal information is unknown. To observe the dynamics of the battery while performing fast charging, many electrochemical model-based closed-loop charging strategies have been proposed [3]–[5], aiming to prevent violating health-related constraints and increase the charging speed at the same time. However, the complexity of the electrochemical model limits its use because of high computation demand, which is a main obstacle to using these strategies practically [6]. To avoid the high computational load in the aforementioned optimization-based strategies, a model inversion-based output tracking control method [7] has been proposed to derive analytical solutions to the

requested output tracking problems in lithium-ion batteries.

The above-mentioned model-based algorithms usually require the model parameters to be well-identified to achieve high control accuracy. One of the most accurate models is the electrochemical pseudo-two-dimensional (P2D) model, which is a complex, high-dimensional, nonlinear partial algebraic-differential equation system [8]. The P2D model is built from the underlying physical understanding of the reaction, diffusion, and migration phenomena that take place inside the batteries, making it possible to predict the internal behaviors, e.g., degradation, of the batteries during charging and discharging. However, since the P2D model consists of around a hundred parameters in a series of coupled partial differential equations, it is inconvenient to use in practice for online battery management. To reduce the complexity of the electrochemical model without losing the ability to predict aging behaviors, the single particle model (SPM) was introduced, which assumes only one particle in each electrode and no electrolyte dynamics [9]. With the simplified model structure, the number of parameters needed to be identified is significantly reduced. However, when using the SPM for battery fast charging design, a major challenge is that the uncertainty in the identified parameters can have considerable influence on the efficacy of the designed charging control scheme [10]. An analysis of a simple electrochemical model with inevitable inaccurate parameters for reliable fast charging control design has not been previously reported.

In this paper, we investigate this problem by designing an inversion-based charging control algorithm for battery charging, which takes into account the parameter bias of the SPM. With this method, the unwanted lithium-plating caused by inaccurate model parameters can be completely avoided, providing the error bounds of the parameters hold. In Section II, we present a reduced SPM with grouped model parameters. In Section III, the details of the SPM-inversion-based output tracking control method are introduced. In Section IV, the safety margin to prevent lithium-plating from occurring is calculated. The results of the proposed SPM-inversion-based control with and without the safety margin are shown, along with a sensitivity analysis of the grouped parameters. Conclusions are given in Section VI.

This work was supported by the Swedish Energy Agency (Grant No. P42787-1) and Swedish Innovation Agency (Grant No. 2019-03402).

All the authors are with the Department of Electrical Engineering, Chalmers University of Technology, Gothenburg, 41296, Sweden (E-mails: yao.cai@chalmers.se; yangli@ieee.org; tw@chalmers.se).

## II. SINGLE PARTICLE MODEL AND MODEL REDUCTION

### A. Single Particle Model

The SPM is a simplified electrochemical model of lithium-ion batteries. Assuming only one solid particle exists in each electrode and no electrolyte dynamics are present, the system order and the number of model parameters are both greatly reduced. The SPM under investigation is given by

$$\frac{\partial \bar{c}_i}{\partial t} = \frac{1}{\theta'_{i1}} \frac{1}{\bar{r}_i^2} \frac{\partial}{\partial \bar{r}_i} \left( \bar{r}_i^2 \frac{\partial \bar{c}_i}{\partial \bar{r}_i} \right), \quad (1)$$

$$\left. \frac{\partial \bar{c}_i}{\partial \bar{r}_i} \right|_{\bar{r}_i=0} = 0, \quad \left. \frac{\partial \bar{c}_i}{\partial \bar{r}_i} \right|_{\bar{r}_i=1} = -\theta'_{i2} I, \quad (2)$$

$$\eta_i = \frac{2RT}{F} \sinh^{-1} \left( \theta'_{i3} \frac{I}{\sqrt{\bar{c}_i^{ss} (1 - \bar{c}_i^{ss})}} \right), \quad (3)$$

$$V = \mathcal{U}_p(\bar{c}_p^{ss}) + \eta_p - \mathcal{U}_n(\bar{c}_n^{ss}) - \eta_n, \quad (4)$$

$$\eta_{\text{LiP}} = \mathcal{U}_n(\bar{c}_n^{ss}) + \eta_n. \quad (5)$$

where  $i \in \{p, n\}$  represents the positive and negative electrodes. Here, (1) governs the diffusion of lithium species in the particles according to the Fick's law, where  $\bar{c}_p$  and  $\bar{c}_n$  are the normalized lithium-ion concentration in the positive and negative electrodes, and  $\bar{r}_p$  and  $\bar{r}_n$  represent the normalized radial position of the two particles, respectively. Equation (2) is the respective boundary conditions of (1), where  $I$  is the current density. Equation (3) is the activation overpotential in the electrode, calculated using the Butler-Volmer equation for reaction kinetics, where  $R$  is the universal gas constant,  $F$  is the Faraday constant,  $T$  is the battery temperature, and  $\bar{c}_i^{ss}$  is the normalized concentration at the surface of the particle. Equation (4) calculates the battery voltage, where  $\mathcal{U}_i$  is the open-circuit potential (OCP) of the electrode, which is a nonlinear function of  $\bar{c}_i^{ss}$ . In (5),  $\eta_{\text{LiP}}$  is the lithium-plating potential. If  $\eta_{\text{LiP}}$  drops below zero, this indicates that lithium-plating has occurred in the negative electrode. Furthermore, Grouped parameters are defined as [11]

$$\theta' = \begin{bmatrix} \theta'_{p1} \\ \theta'_{p2} \\ \theta'_{p3} \\ \theta'_{n1} \\ \theta'_{n2} \\ \theta'_{n3} \end{bmatrix} = \begin{bmatrix} \frac{R_p^2}{D_p} \\ -\frac{R_p^2}{D_p} \frac{1}{3\epsilon_p L_p c_p^{\max} F A} \\ -\frac{R_p}{2k_p \sqrt{c_e}} \frac{1}{3\epsilon_p L_p c_p^{\max} F A} \\ \frac{R_n^2}{D_n} \\ \frac{R_n^2}{D_n} \frac{1}{3\epsilon_n L_n c_n^{\max} F A} \\ \frac{R_n}{2k_n \sqrt{c_e}} \frac{1}{3\epsilon_n L_n c_n^{\max} F A} \end{bmatrix}, \quad (6)$$

and the meaning of the symbols are given in the appendix.

### B. Padé Approximation

To simplify the PDEs in the SPM, the Padé approximation is applied [12], [13]. Instead of the concentration variables concerning the position and the time inside the PDE, the normalized surface concentration  $\bar{c}_i^{ss}$ , the normalized volume-averaged concentration  $\bar{c}_i^{\text{avg}}$ , and a set of concentration deviation terms are used to represent the normalized lithium-ion concentration dynamics. Considering the 2nd-order Padé approximation with a normalized concentration in the negative

electrode, a reduced negative electrode model is

$$\frac{d\bar{c}_n^{\text{avg}}(t)}{dt} = -3\theta_{n1} I(t) \quad (7)$$

$$\frac{d\bar{c}_n^{\text{diff}}(t)}{dt} = -\frac{35}{\theta_{n1}} \bar{c}_n^{\text{diff}}(t) - 7\theta_{n2} I(t) \quad (8)$$

$$\bar{c}_n^{ss}(t) = \bar{c}_n^{\text{avg}}(t) + \bar{c}_n^{\text{diff}}(t), \quad (9)$$

where  $\theta_{n1}$  and  $\theta_{n2}$  are two redefined grouped parameters for the convenience of further analysis:

$$\begin{bmatrix} \theta_{n1} \\ \theta_{n2} \end{bmatrix} = \begin{bmatrix} \frac{R_n^2}{D_n} \\ \frac{1}{3\epsilon_n L_n c_n^{\max} F A} \end{bmatrix}. \quad (10)$$

Given the initial averaged concentration  $\bar{c}_n^{\text{avg}}(0)$  and assuming the initial  $\bar{c}_n^{\text{diff}}(0) = 0$ , (7)–(9) can be solved as

$$\bar{c}_n^{\text{avg}}(t) = \bar{c}_n^{\text{avg}}(0) - 3\theta_{n2} \int_0^t I(t') dt' \quad (11)$$

$$\bar{c}_n^{\text{diff}}(t) = -\frac{I(t)\theta_{n1}\theta_{n2}}{5} + \frac{I(t)\theta_{n1}\theta_{n2}e^{-\frac{35t}{\theta_{n1}}}}{5} \quad (12)$$

$$\begin{aligned} \bar{c}_n^{ss}(t) &= \bar{c}_n^{\text{avg}}(0) - 3\theta_{n2} \int_0^t I(t') dt' - \frac{I(t)\theta_{n1}\theta_{n2}}{5} \\ &+ \frac{I(t)\theta_{n1}\theta_{n2}e^{-\frac{35t}{\theta_{n1}}}}{5} \end{aligned} \quad (13)$$

The overpotential in the negative electrode is

$$\eta_n = \frac{2RT}{F} \sinh^{-1} \left( \theta_{n3} \frac{I}{\sqrt{\bar{c}_n^{ss} (1 - \bar{c}_n^{ss})}} \right), \quad (14)$$

where  $\theta_{n3} = \theta'_{n3}$ .

A similar result can be derived for the positive electrode. The new grouped parameters are

$$\theta = \begin{bmatrix} \theta_{p1} \\ \theta_{p2} \\ \theta_{p3} \\ \theta_{n1} \\ \theta_{n2} \\ \theta_{n3} \end{bmatrix} = \begin{bmatrix} \frac{R_p^2}{D_p} \\ -\frac{1}{3\epsilon_p L_p c_p^{\max} F A} \\ -\frac{R_p}{2k_p \sqrt{c_e}} \frac{1}{3\epsilon_p L_p c_p^{\max} F A} \\ \frac{R_n^2}{D_n} \\ \frac{1}{3\epsilon_n L_n c_n^{\max} F A} \\ \frac{R_n}{2k_n \sqrt{c_e}} \frac{1}{3\epsilon_n L_n c_n^{\max} F A} \end{bmatrix}. \quad (15)$$

## III. SPM-INVERSION-BASED OUTPUT TRACKING CONTROL METHOD

In general, the charging current needs to be as high as possible to shorten the charging time. However, too large current will cause lithium-plating, attributed to a negative  $\eta_{\text{LiP}}$ . Therefore, in order to avoid Li-plating while fast charging,  $\eta_{\text{LiP}}$  needs to be limited at a non-negative value, i.e.,

$$\eta_{\text{LiP}} = \mathcal{U}_n(\bar{c}_n^{ss}) + \eta_n = \eta_{\min} \geq 0, \quad (16)$$

where  $\eta_{\min}$  is the safety margin set for the lithium-plating overpotential, which is a non-negative value. When  $\eta_{\text{LiP}}$  falls below zero, this indicates that lithium deposition has occurred. The purpose of the inversion-based output tracking control method is to calculate the maximum instantaneous input current that can satisfy (16).

Inserting (14) into (16), it can be derived that

$$I = \sinh\left(\left(\eta_{\min} - \mathcal{U}_n(\bar{c}_n^{ss})\right) \frac{F}{2RT}\right) \frac{\sqrt{\bar{c}_n^{ss}(1 - \bar{c}_n^{ss})}}{\theta_{n3}}. \quad (17)$$

Note that a constant current charging stage is usually applied at the beginning of the charging process, and this current limit is denoted as  $I_c$ . The calculated input current in (17) will only be adopted when it is smaller than the limit  $I_c$ , and thus the final applied input current, denoted by  $I_{app}$ , is

$$I_{app} = \min(|I|, |I_c|). \quad (18)$$

Equation (18) gives the exact solution to achieve constant-current constant-potential (CC-C $\eta$ ) charging for the reduced SPM. In practice, since true model states and parameters are unknown, this current can only be calculated from the estimated states and identified model parameters, i.e.,  $\hat{\mathcal{U}}_n$ ,  $\hat{c}_n^{ss}$  and  $\hat{\theta}_{n3}$ . The process can be described in Fig. 1.

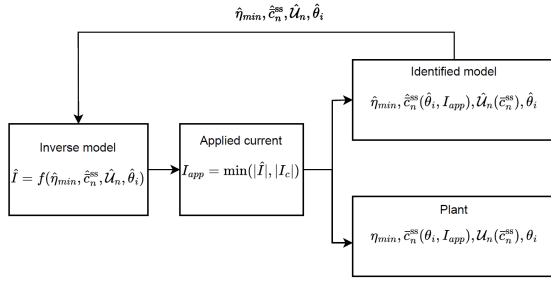


Fig. 1. Inversion-based control based on the identified model.

Fig. 1 shows that the parameters and states needed to calculate the applied current are calculated from the identified model. Due to the unavoidable parameter errors, a safety margin must be introduced to avoid lithium-plating. Denote  $\hat{\eta}_{\min}$  as the applied limit in the inverse model and  $\eta_{\min}$  as the limit set for the plant. When choosing  $\hat{\eta}_{\min} = \eta_{\min}$ , the applied current can only prevent the battery from lithium-plating if the model is the same as the battery plant.

#### IV. CALCULATION OF SAFETY MARGIN

In the rest of the work, plant parameters are denoted by

$$[\theta_{p1}, \theta_{p2}, \theta_{p3}, \theta_{n1}, \theta_{n2}, \theta_{n3}]$$

and the corresponding estimated parameters by

$$[\hat{\theta}_{p1}, \hat{\theta}_{p2}, \hat{\theta}_{p3}, \hat{\theta}_{n1}, \hat{\theta}_{n2}, \hat{\theta}_{n3}]$$

The relationships between the true and estimated parameters are expressed by

$$\theta_{ik} = (1 + q_{ik})\hat{\theta}_{ik}, \quad (19)$$

where  $i \in \{p, n\}$ ,  $k \in \{1, 2, 3\}$ .  $q_{ik}$  represents the normalized difference between the corresponding true and estimated parameter.

#### A. With Known Parameter Bias

We start our investigation assuming known parameter bias. This calculation serves as theoretical analysis of the influence of parameter errors on the charging performance, and it is a base for the next step where the safety margin for a known range of parameter bias can be calculated.

In the rest of the work, the superscript “ss” that represents the surface concentration of the solid phase particle is dropped for ease of notation.

For a battery model with a differentiable negative-electrode OCP function, the estimated negative OCP is expressed as

$$\hat{\mathcal{U}}_n = F_n(\hat{c}_n)$$

Similarly, the plant’s OCP is

$$\mathcal{U}_n = F_n(\bar{c}_n).$$

We define

$$\Delta\bar{c}_n = \hat{c}_n - \bar{c}_n$$

It can then be derived that

$$\begin{aligned} \Delta\bar{c}_n(t) = \hat{c}_n(t) - \bar{c}_n(t) &= 3q_{n2}\hat{\theta}_{n2} \int_0^t I(t')dt' + \\ &\frac{I(t)}{5} [\hat{\theta}_{n1}\hat{\theta}_{n2}(e^{-\frac{35t}{\hat{\theta}_{n1}}} - 1) - \theta_{n1}\theta_{n2}(e^{-\frac{35t}{\theta_{n1}}} - 1)]. \end{aligned} \quad (20)$$

where  $e^{-\frac{35t}{\hat{\theta}_{n1}}}$  and  $e^{-\frac{35t}{\theta_{n1}}}$  quickly drop towards zero as  $t$  increases. Thus, using (19), we have

$$\begin{aligned} \Delta\bar{c}_n(t) &\approx 3q_{n2}\hat{\theta}_{n2} \int_0^t I(t')dt' \\ &+ \frac{I(t)}{5} (q_{n1} + q_{n2} + q_{n1}q_{n2})\hat{\theta}_{n1}\hat{\theta}_{n2}, \end{aligned} \quad (21)$$

which shows that  $\Delta\bar{c}_n$  is a function of  $q_{n1}$  and  $q_{n2}$ .

Applying a first-order Taylor’s expansion, we have

$$F_n(\bar{c}_n) = F_n(\hat{c}_n) + F'_n(\hat{c}_n)(\bar{c}_n - \hat{c}_n), \quad (22)$$

and

$$\mathcal{U}_n = \hat{\mathcal{U}}_n - F'_n(\hat{c}_n)\Delta\bar{c}_n = \hat{\mathcal{U}}_n + \Delta_{n1}, \quad (23)$$

where

$$\Delta_{n1} = -F'_n(\hat{c}_n)\Delta\bar{c}_n. \quad (24)$$

For the negative overpotential, the estimated and true values are denoted as

$$\hat{\eta}_n = Y_n(\hat{c}_n, \hat{\theta}_{n3})$$

$$\eta_n = Y_n(\bar{c}_n, \theta_{n3}).$$

Denote the partial derivatives of  $Y_n(\hat{c}_n, \hat{\theta}_{n3})$  with respect to  $\hat{c}_n$  and  $\hat{\theta}_{n3}$  as  $Y'_{n,\hat{c}_n}(\hat{c}_n, \hat{\theta}_{n3})$  and  $Y'_{n,\hat{\theta}_{n3}}(\hat{c}_n, \hat{\theta}_{n3})$  respectively.

Also define

$$\Delta\theta_{n3} = \hat{\theta}_{n3} - \theta_{n3} = -q_{n3}\hat{\theta}_{n3}.$$

Once more, using a first-order Taylor’s expansion,

$$\begin{aligned} Y_n(\bar{c}_n, \theta_{n3}) &= Y_n(\hat{c}_n, \hat{\theta}_{n3}) + Y'_{n,\hat{c}_n}(\hat{c}_n, \hat{\theta}_{n3})(\bar{c}_n - \hat{c}_n) \\ &+ Y'_{n,\hat{\theta}_{n3}}(\hat{c}_n, \hat{\theta}_{n3})(\theta_{n3} - \hat{\theta}_{n3}) \end{aligned} \quad (25)$$

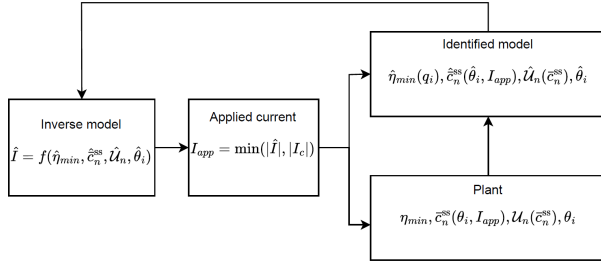


Fig. 2. Inversion-based control with safety margin.

$$\begin{aligned} \eta_n &= \hat{\eta}_n - Y'_{n, \hat{c}_n}(\hat{c}_n, \hat{\theta}_{n3}) \Delta \bar{c}_n - Y'_{n, \hat{\theta}_{n3}}(\hat{c}_n, \hat{\theta}_{n3}) \Delta \theta_{n3} \\ &= \hat{\eta}_n + \Delta_{n2}, \end{aligned} \quad (26)$$

where

$$\Delta_{n2} = -Y'_{n, \hat{c}_n}(\hat{c}_n, \hat{\theta}_{n3}) \Delta \bar{c}_n - Y'_{n, \hat{\theta}_{n3}}(\hat{c}_n, \hat{\theta}_{n3}) \Delta \theta_{n3}. \quad (27)$$

With  $\Delta_{n2}$  and  $\Delta_{n1}$ , the next step is to find the relationship between  $\hat{\eta}_{\text{LiP}}$  and  $\eta_{\text{LiP}}$ , we have

$$\begin{aligned} \eta_{\text{LiP}} &= \mathcal{U}_n + \eta_n \\ &= (\hat{\mathcal{U}}_n + \Delta_{n1}) + (\hat{\eta}_n + \Delta_{n2}) \\ &= \hat{\eta}_{\text{LiP}} + \Delta_{n1} + \Delta_{n2}, \end{aligned} \quad (28)$$

Now, let  $\hat{\eta}_{\text{LiP}} = \hat{\eta}_{\text{min}}$  and  $\eta_{\text{LiP}} = \eta_{\text{min}}$ , which gives,

$$\hat{\eta}_{\text{min}} = \eta_{\text{min}} - \Delta_{n1} - \Delta_{n2}, \quad (29)$$

Equation (29) suggests that in order to achieve lithium-plating-free charging control, i.e.,  $\eta_{\text{min}} = 0$ , the safety margin should be set to  $-(\Delta_{n1} + \Delta_{n2})$ . The whole process of calculating this safety margin is summarized in Fig. 2. Compared to Fig. 1, the difference is that parameter biases exist in Fig. 2, and these biases are assumed to be known. With this information, the required safety margin for zero-lithium-plating charging,  $\hat{\eta}_{\text{min}}$ , can be calculated. For the inversion-based charging control, the applied current calculated based on  $\hat{\eta}_{\text{min}}$  will prevent the cell from triggering lithium-plating. We summarize the control strategy in Fig. 2 as Algorithm 1.

### B. With Known Parameter Bias Range

In practice, the parameter bias cannot be known precisely. A most realistic situation is that the range of the bias is available [11], [14]. In this case, the safety margin should be selected so that no possible parameter bias combinations of  $q_{n1}$ ,  $q_{n2}$ , and  $q_{n3}$ , will lead to lithium-plating during the charging process.

As mentioned earlier,  $\Delta \bar{c}_n$  is a function of  $q_{n1}$  and  $q_{n2}$ . Assuming  $-1 < q_{n1}, q_{n2}, q_{n3} < 1$ , the derivative of  $\Delta \bar{c}_n$  with respect to  $q_{n1}$  and  $q_{n2}$  can be derived as

$$\frac{\partial \Delta \bar{c}_n}{\partial q_{n1}} = \frac{I(t)}{5} \hat{\theta}_{n1} \hat{\theta}_{n2} (1 + q_{n2}) < 0 \quad (30)$$

$$\frac{\partial \Delta \bar{c}_n}{\partial q_{n2}} = 3 \hat{\theta}_{n2} \int_0^t I(t') dt' + \frac{I(t)}{5} \hat{\theta}_{n1} \hat{\theta}_{n2} (1 + q_{n1}) < 0. \quad (31)$$

**Algorithm 1** Find the safety margin with known parameter bias values

**Input**  $tol = 1 \times 10^{-9}$ ,  $\eta_{\text{min}} = 0$ ,  $\hat{\theta}_i$ ,  $\hat{q}_i$ , and  $I_c$

**Output**  $\hat{\eta}_{\text{min}}$  and  $I_{\text{app}}$

- 1: Initialize  $\hat{\eta}_{\text{min}} = \eta_{\text{min}} - 0.1$ ;
- 2: **for** each iteration **do**
- 3:    $\hat{\eta}_{\text{min}}^{\text{pre}} = \hat{\eta}_{\text{min}}$
- 4:   **for** each time sample **do**
- 5:     Calculate model-inversion-based current
- 6:      $\hat{I} = f(\hat{\eta}_{\text{min}})$ ,
- 7:      $I_{\text{app}} = \max(|I_c|, |\hat{I}|)$
- 8:   **end for**
- 9:   Calculate time-dependent  $\hat{\eta}_{\text{min}}(t)$  series by (24), (27), and (29);
- 10:    $\hat{\eta}_{\text{min}} = \max(\hat{\eta}_{\text{min}}(t_{\text{inv}} : t_{\text{end}}))$ , where  $t_{\text{inv}}$  is the time when  $\hat{I}$  starts to be effective;
- 11:   **if**  $\|\hat{\eta}_{\text{min}}^{\text{pre}} - \hat{\eta}_{\text{min}}\|_{\infty} < tol$  **then**
- 12:     **break**
- 13:   **end if**
- 14: **end for**

The derivative of  $\Delta_{n1}$  with respect to  $q_{n1}$  and  $q_{n2}$  can thus be derived as

$$\frac{\partial \Delta_{n1}}{\partial q_{ik}} = \frac{d \Delta_{n1}}{d \Delta \bar{c}_n} \frac{\partial \Delta \bar{c}_n}{\partial q_{ik}} = -F'_n(\hat{c}_n) \frac{\partial \Delta \bar{c}_n}{\partial q_{ik}}, ik \in \{n1, n2\} \quad (32)$$

The deviation of  $\Delta_{n2}$  with respect to  $q_{n1}$ ,  $q_{n2}$ , and  $q_{n3}$  can also be, and the results are derived, yielding:

$$\begin{aligned} \frac{\partial \Delta_{n2}}{\partial q_{ik}} &= \frac{\partial \Delta_{n2}}{\partial \Delta \bar{c}_n} \frac{\partial \Delta \bar{c}_n}{\partial q_{ik}} \\ &= -Y'_{n, \hat{c}_n}(\hat{c}_n, \hat{\theta}_{n3}) \frac{\partial \Delta \bar{c}_n}{\partial q_{ik}}, ik \in \{n1, n2\} \end{aligned} \quad (33)$$

$$\frac{\partial \Delta_{n2}}{\partial q_{n3}} = \frac{\partial \Delta_{n2}}{\partial \Delta \theta_{n3}} \frac{\partial \Delta \theta_{n3}}{\partial q_{n3}} = Y'_{n, \hat{\theta}_{n3}}(\hat{c}_n, \hat{\theta}_{n3}) \hat{\theta}_{n3} \quad (34)$$

Here, the functions  $F'_n(\hat{c}_n)$ ,  $Y'_{n, \hat{c}_n}(\hat{c}_n, \hat{\theta}_{n3})$ , and  $Y'_{n, \hat{\theta}_{n3}}(\hat{c}_n, \hat{\theta}_{n3})$  can be derived from the expressions of  $\mathcal{U}_n$  and  $\hat{\eta}_n$ . Consequently, the derivatives of the safety margin w.r.t. the parameter biases can be calculated. Hence, the adjustment of the safety margins can be performed if the range of the parameter is provided. This can help to find out the maximum possible safety margin, which can prevent lithium-plating for all the possible parameter variations within the given range.

## V. RESULTS AND DISCUSSION

Simulations were conducted to verify the proposed method to determine the safety margin for battery charging control. The battery parameters are for a cylindrical 21700 commercial cell (LGM50) [15]. Furthermore, the range of the parameter biases are limited to

$$q_{ik} \in [-0.1, 0.1], i \in \{p, n\}, k \in \{1, 2, 3\} \quad (35)$$

### A. Verification of the SPM-Inversion-Based Fast Charging Method

Fig. 3 shows an example of the simulation result of the SPM-inversion-based control. For demonstration purposes, we select  $\hat{\eta}_{\min} = 20$  mV, upon which the control current is calculated and shown. In this example, the true model parameters are used in the controller design. It can be seen that at the beginning of the simulation, the constant charging rate 1.5C is applied while  $\hat{\eta}_{LiP}$  begins to decrease. When  $\hat{\eta}_{LiP}$  drops to the preset  $\hat{\eta}_{\min}$ , the applied current begins to decrease since the inversion-based control is triggered at the same moment. After that, it is shown that  $\hat{\eta}_{LiP}$  can follow  $\hat{\eta}_{\min}$  well by applying the calculated current.

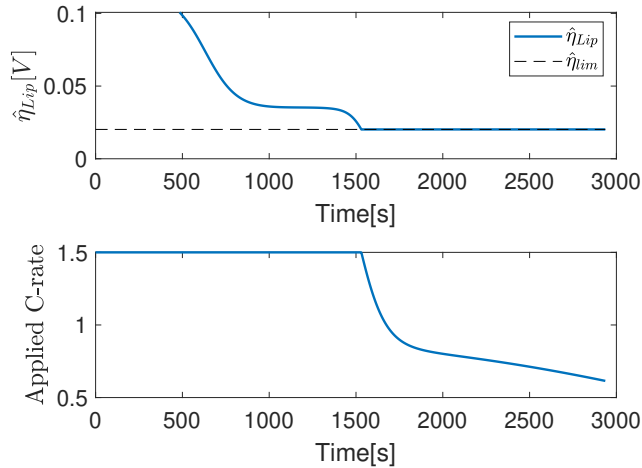


Fig. 3.  $\hat{\eta}_{LiP}$  and applied C-rate under SPM inversion-based control. Here  $\hat{\eta}_{lim} \equiv \hat{\eta}_{\min}$ .

### B. Verification of the Calculated Safety Margin

When there is a parameters bias, if no safety margin is set for the model, i.e.,  $\hat{\eta}_{\min} = 0$  V, lithium-plating can happen in the plant when performing the SPM-inversion-based control. In Fig. 4, 1000 random simulations were tested. In each simulation, again, 1.5C constant current was applied at the beginning of the charging, and the control current calculated from the inversion-based method is applied at the moment when it drops below 1.5C. Parameter biases were generated randomly within the predefined range,  $q_{ik} \in [-0.1, 0.1]$ , in each simulation. The simulation results show that some parameter biases can lead to negative  $\eta_{LiP}$ , which indicates that lithium-plating has occurred.

Next, we apply the proposed Algorithm 1 for 1000 random simulations. In each simulation, a random parameter set  $[q_{n1}, q_{n2}, q_{n3}, q_{ik} \in [-0.1, 0.1]]$ , is assigned to the plant. With (24), (27), and (29), a specific safety margin  $\hat{\eta}_{\min}$  can be calculated. Similarly, in the constant charging period, the current is selected as 1.5C, and the control current calculated under the new safety margin is derived and compared with the constant current, the smaller one will be applied. In each simulation, the parameter bias is known. With the calculated safety margin, 1000  $\eta_{LiP}$  curves from the plant

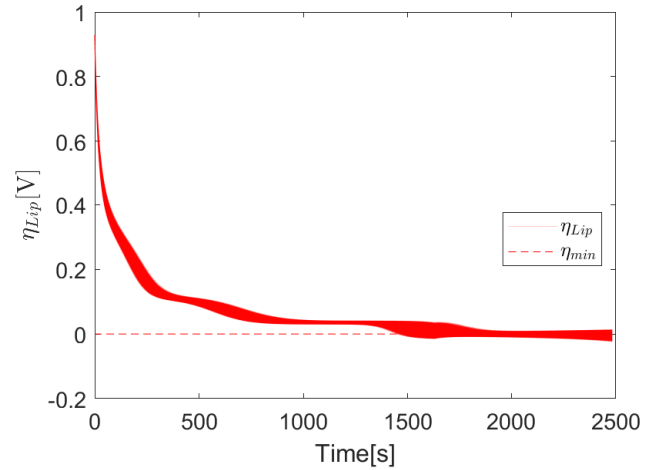


Fig. 4.  $\eta_{LiP}$  in 1000 simulations with  $\hat{\eta}_{\min} = 0$  V and random parameter bias.

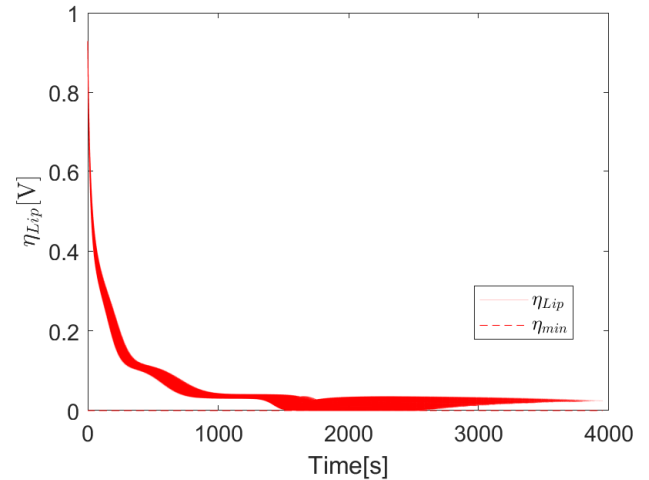


Fig. 5.  $\eta_{LiP}$  in 1000 simulations using Algorithm 1. Parameter bias is known.

are illustrated in Fig. 5. Every line corresponds to a randomly generated parameter set bias within the limit and a specifically calculated safety margin. We plot the histogram of the minimum value of  $\eta_{LiP}$  in all these simulations in Fig. 6, from which it can be seen that all the deviations are positive, meaning no lithium-plating occurs. This shows that in all the 1000 cases Algorithm 1 works well. The calculated maximum safety margin among all the simulations is 0.0422 V. It approaches but remains below the calculated theoretical value of 0.0431 V.

It should be noted that, in Fig. 4, the minimum value of  $\eta_{LiP}$  is found to be  $-0.023$  V in all these cases, but this does not mean the safety margin needs to be set at 0.023 V since changing the safety margin can affect the entire current trajectory, possibly still causing lithium-plating. In order to demonstrate this, we compare the results between the cases with safety margin  $\hat{\eta}_{\min} = 0.023$  V and  $\hat{\eta}_{\min} = 0.0431$  V in Figs. 7 and 8. In Fig. 7, the red dashed line is the safety

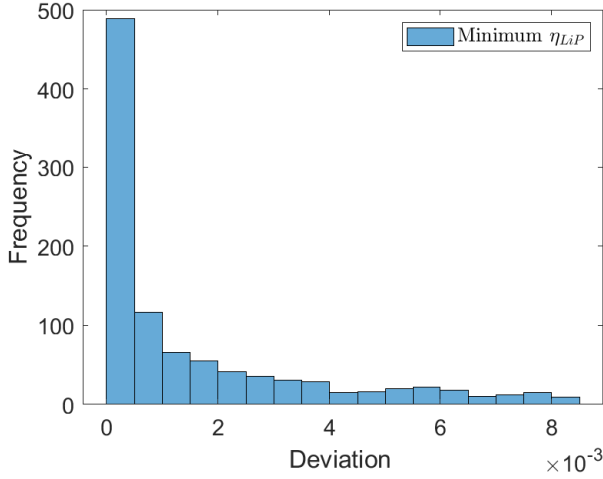


Fig. 6. Histogram of minimum value of  $\eta_{LiP}$  in Fig. 5.

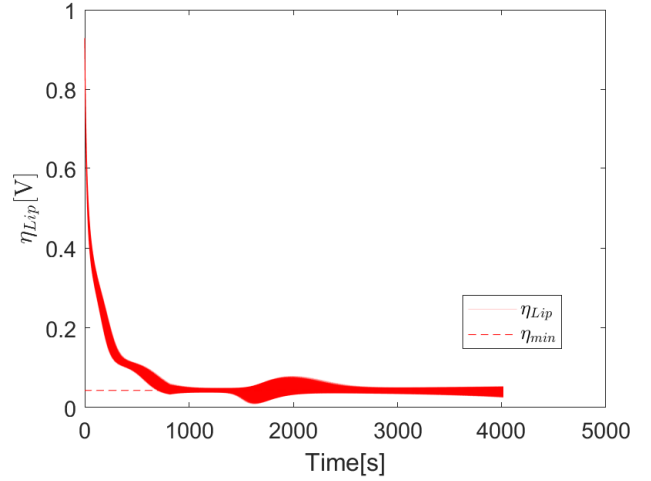


Fig. 8.  $\eta_{LiP}$  in 1000 simulations with  $\hat{\eta}_{min} = 0.0431$  V and random parameter bias.

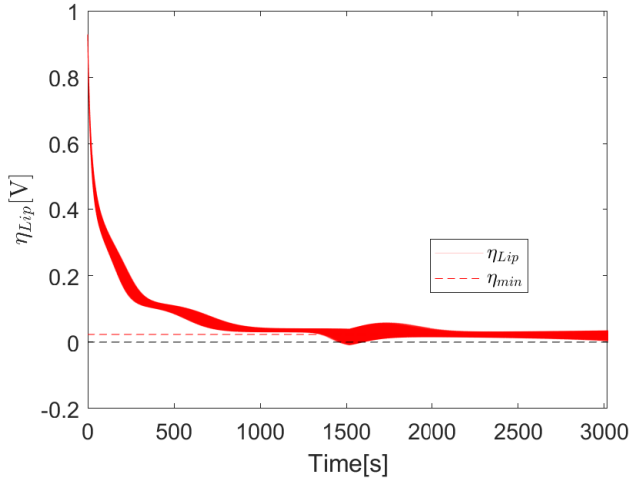


Fig. 7.  $\eta_{LiP}$  in 1000 simulations with  $\hat{\eta}_{min} = 0.023$  V and random parameter bias.

margin  $\hat{\eta}_{min} = 0.023$  V, and the black dashed line is zero. It can be seen that there are many cases in which the lithium-plating potential drops below zero. In contrast, in Fig. 8, all the lines are above zero and the lowest points are close to zero. This indicates that with the proposed method, it is possible to achieve lithium-plating-free charging with a small safety margin.

### C. Sensitivity Analysis

From (30), it can be seen that  $q_{n2}$  is the coefficient of the integration of the current, which means  $q_{n2}$  is the dominant term that can affect the safety margin. A sensitivity analysis is carried out on the safety margin, the mean abstract error of the output voltage, and the maximum error of the output voltage. The normalized results of the sensitivity analysis on  $q_{n1}, q_{n2}, q_{n3}, q_{p1}, q_{p2},$  and  $q_{p3}$  are shown in Fig. 9. For the safety margin, it is  $q_{n2}$  that dominates, whereas for the voltage error,  $q_{p2}$  is much more sensitive to other parameters.

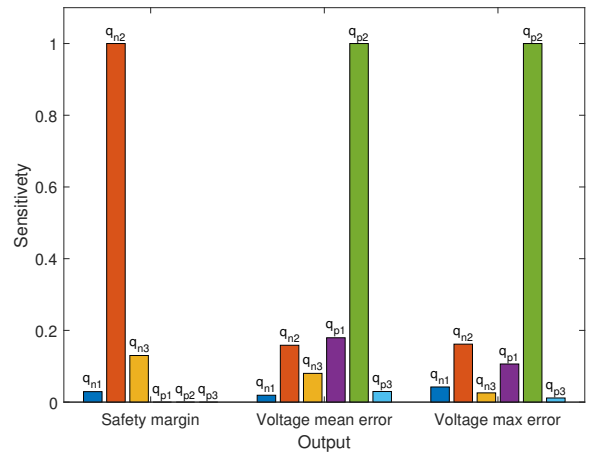


Fig. 9. Sensitivity analysis on  $q_{n1}, q_{n2}, q_{n3}, q_{p1}, q_{p2},$  and  $q_{p3}$  with respect to different output.

## VI. CONCLUSION

Several concluding remarks are given as follows. Firstly, SPM inversion-based control may cause lithium-plating in the Li-ion battery if no safety margin is set. To find a suitable safety margin, only running Monte Carlo simulations to find the minimum possible  $\eta_{LiP}$  does not work.

Algorithm 1 is developed to calculate the theoretical safety margin. When the range of the parameter bias is known, we can calculate the safety margin that works under all the parameter biases. The Monte Carlo simulation result is also given to verify the theoretical result.

Besides, the theoretical safety margin is verified by simulations. The final results show that the safety margin is large enough to prevent Li-plating in all the simulations while small enough to be not wasted.

Finally, the sensitivity analysis shows that the safety margin is most and much more sensitive to  $q_{n2}$  than to other parameter biases while the voltage mean error and maximum

error are most sensitive to  $q_{p2}$ . Therefore, in our future work, the deviation of the terminal voltage can be considered in the calculation of the safety margin. In addition, it can be seen at the late stage of charging, the safety margin is higher than needed, which implies that a hybrid fast-charging control method can be developed for shorter charging time.

#### APPENDIX

$c_i$ : Solid-phase concentration [ $\text{mol} \cdot \text{m}^{-3}$ ]  
 $c_i^{\text{avg}}$ : Volume-averaged solid-phase concentration [ $\text{mol} \cdot \text{m}^{-3}$ ]  
 $c_i^{\text{max}}$ : Theoretical maximum solid-phase concentration [ $\text{mol} \cdot \text{m}^{-3}$ ]  
 $c_i^{\text{ss}}$ : Surface concentration of solid-particle [ $\text{mol} \cdot \text{m}^{-3}$ ]  
 $c_i^{\text{diff}}$ : Concentration difference between  $c_i^{\text{avg}}$  and  $c_i^{\text{ss}}$  [ $\text{mol} \cdot \text{m}^{-3}$ ]  
 $c_e$ : Electrolyte concentration [ $\text{mol} \cdot \text{m}^{-3}$ ]  
 $R_i$ : Radius of the solid-phase particle [m]  
 $L_i$ : Thickness of the electrode [m]  
 $D_i$ : Solid-phase diffusion coefficient [ $\text{m}^2 \cdot \text{s}^{-1}$ ]  
 $\varepsilon_i$ : Volume fraction of the solid phase [-]  
 $k_i$ : Reaction rate [ $\text{A} \cdot \text{m}^{2.5} \cdot \text{mol}^{-1.5}$ ]  
 $U_i$ : Open-circuit potential of the electrode [V]  
 $\eta_i$ : Activation overpotential for intercalation [V]  
 $\eta_{\text{min}}$ : Limit for the Li-plating overpotential [V]  
 $I_{\text{app}}$ : Applied current to the model and plant [A]  
 $I_c$ : Constant charging stage current [A]  
 $A$ : Electrode plate area [ $\text{m}^2$ ]  
 $F$ : Faraday constant [ $\text{s} \cdot \text{A} \cdot \text{mol}^{-1}$ ]  
 $T$ : Cell temperature [K]  
 $R$ : Universal gas constant [ $\text{J} \cdot \text{K}^{-1} \cdot \text{mol}^{-1}$ ]  
 $i = p$ : Positive electrode  
 $i = n$ : Negative electrode  
 $\bar{x}$ : Normalized value of  $x$   
 $\hat{x}$ : Estimated value of  $\bar{x}$

#### REFERENCES

- [1] J. S. Edge, S. O’Kane, R. Prosser, N. D. Kirkaldy, A. N. Patel, A. Hales, A. Ghosh, W. Ai, J. Chen, J. Yang *et al.*, “Lithium ion battery degradation: what you need to know,” *Phys. Chem. Chem. Phys.*, vol. 23, no. 14, pp. 8200–8221, 2021.
- [2] B. Arabsalmanabadi, N. Tashakor, A. Javadi, and K. Al-Haddad, “Charging techniques in lithium-ion battery charger: Review and new solution,” in *Proc. Annual Conf. IEEE Ind. Electron. Soc. (IECON)*, 2018, pp. 5731–5738.
- [3] F. Ringbeck, M. Garbade, and D. U. Sauer, “Uncertainty-aware state estimation for electrochemical model-based fast charging control of lithium-ion batteries,” *J. Power Sources*, vol. 470, p. 228221, 2020.
- [4] Z. Chu, X. Feng, L. Lu, J. Li, X. Han, and M. Ouyang, “Non-destructive fast charging algorithm of lithium-ion batteries based on the control-oriented electrochemical model,” *Appl. Energy*, vol. 204, pp. 1240–1250, 2017.
- [5] Y. Li, D. M. Vilathgamuwa, E. Wikner, Z. Wei, X. Zhang, T. Thiringer, T. Wik, and C. Zou, “Electrochemical model-based fast charging: Physical constraint-triggered PI control,” *IEEE Trans. Energy Convers.*, vol. 36, no. 4, pp. 3208–3220, Dec. 2021.
- [6] Y. Li, D. Karunathilake, D. M. Vilathgamuwa, Y. Mishra, T. W. Farrell, S. S. Choi, and C. Zou, “Model order reduction techniques for physics-based lithium-ion battery management: A survey,” *IEEE Ind. Electron. Mag.*, vol. 16, no. 3, pp. 36–51, Sep. 2022.
- [7] Y. Li, T. Wik, Y. Huang, and C. Zou, “Nonlinear model inversion-based output tracking control for battery fast charging,” *IEEE Trans. Control Syst. Technol.*, vol. 32, no. 1, pp. 225–240, 2024.
- [8] V. Laue, F. Röder, and U. Kreuer, “Practical identifiability of electrochemical P2D models for lithium-ion batteries,” *J. Appl. Electrochem.*, vol. 51, no. 9, pp. 1253–1265, 2021.
- [9] X. Lin, X. Hao, Z. Liu, and W. Jia, “Health conscious fast charging of li-ion batteries via a single particle model with aging mechanisms,” *J. Power Sources*, vol. 400, pp. 305–316, 2018.
- [10] Y. Cai, C. Zou, Y. Li, and T. Wik, “Fast charging control of lithium-ion batteries: Effects of input, model, and parameter uncertainties,” in *Proc. Eur. Control Conf. (ECC)*, 2022, pp. 1647–1653.
- [11] A. M. Bizeray, J. Kim, S. R. Duncan, and D. A. Howey, “Identifiability and parameter estimation of the single particle lithium-ion battery model,” *IEEE Trans. Control Syst. Technol.*, vol. 27, no. 5, pp. 1862–1877, 2019.

- [12] N. T. Tran, M. Vilathgamuwa, T. Farrell, S. S. Choi, Y. Li, and J. Teague, “A Padé approximate model of lithium ion batteries,” *J. Electrochem. Soc.*, vol. 165, no. 7, p. A1409, May 2018.
- [13] J. Basdevant, “The Padé approximation and its physical applications,” *Fortschritte der Physik*, vol. 20, no. 5, pp. 283–331, 1972.
- [14] E. Namor, D. Torregrossa, R. Cherkaoui, and M. Paolone, “Parameter identification of a lithium-ion cell single-particle model through non-invasive testing,” *J. Energy Storage*, vol. 12, pp. 138–148, 2017.
- [15] C.-H. Chen, F. B. Planella, K. O’Regan, D. Gastol, W. D. Widanage, and E. Kendrick, “Development of experimental techniques for parameterization of multi-scale lithium-ion battery models,” *J. Electrochem. Soc.*, vol. 167, no. 8, p. 080534, May 2020.